Dual radio-frequency discharges: Effective frequency concept and effective frequency transition

H. C. Kim and J. K. Lee[a)]
Department of Electronic and Electrical Engineering, Pohang University of Science and Technology, Pohang 790-784, Republic of Korea

(Received 16 July 2004; accepted 18 April 2005; published 7 June 2005)

A concept of effective frequency is introduced to study dual-frequency (DF) capacitively coupled plasmas (CCP) which can be analyzed in a fashion similar to single-frequency (SF) CCP driven with effective parameters. Effective frequencies can be defined quantitatively for ion bombardment energy distribution functions and rf discharge parameters by analyzing ion dynamics in ion-collisionless dual rf sheaths and a homogeneous plasma model for dual rf discharges, respectively. Unlike the driving frequency in SF CCP, the effective frequency in DF CCP is dependent on the ratio of two driving voltages or currents. This characteristic makes it possible to control the ion flux and ion bombardment energy independently. The abrupt transition of the effective frequency leads to several physical phenomena unique in DF CCP. © *2005 American Vacuum Society.* [DOI: 10.1116/1.1931683]

I. INTRODUCTION

Plasma processing is an essential step for manufacturing the ultralarge scale integrated circuits. There are several issues to be resolved in plasma processing using capacitively coupled radio-frequency (rf) discharges, such as the independent control of ion flux and ion bombardment energy, elimination of notch (local sidewall etching), increase of plasma density, and enhancement of etching selectivity and anisotropy. As the device size shrinks with increased aspect ratio, the restrictions become severer. Conventional capacitive reactors with a single rf (13.56 MHz) source have been continuously modified for further improvements of their performance. Dual frequency (DF) capacitively coupled plasma (CCP) operated with an additional power supply driven by a different frequency attracted much attention as a mainstream plasma source for dielectric etchers.[1–8] It has the advantage of the independent control of ion flux and ion bombardment energy, which is crucial for material processing. The physics of DF CCP, however, has not been fully investigated as that of single frequency (SF) CCP. The concept of effective quantities such as quasiparticles with effective mass and pseudopotential in solid state physics[9] has been widely used to reduce complex systems to simpler ones. In the present study, we introduce a concept of effective frequency to understand DF CCP by treating it as SF CCP that is a simpler and well-known system.

When one of two power sources is much stronger than the other, DF CCP acts just as SF CCP driven with the stronger power source. In terms of the effective frequency concept, the effective frequency simply corresponds to the driving frequency of the stronger power source. When the voltage (or current) of the other power source increases, the effective frequency varies from the frequency of the stronger power source to that of the other power source. This is the so-called effective frequency transition. The effective frequency in DF CCP is dependent on the ratio of two driving voltages or currents, unlike the driving frequency in SF CCP: the effective frequency is determined by the competition of two rf sources. This characteristic of DF CCP may lead to physical phenomena that are unique in DF CCP. The effective frequency may vary for different models which have different scaling laws. The advantage of DF CCP comes from the different role of each power source. The high-frequency source is primarily used as the ionization source while the low-frequency source is primarily used for ion acceleration towards the substrate. In terms of the effective frequency concept, the effective frequency for the ionization process corresponds to the higher frequency, while that for the ion energy model corresponds to the lower frequency.

In this article, we report on the possibility of understanding DF CCP just as SF CCP driven with effective parameters. This concept is useful to explain physical issues associated with DF CCP. The analytic model for ion energy distribution (IED) functions in DF CCP is described in Sec. II. The analytic expression for the IED width is obtained by analyzing ion dynamics in ion-collisionless dual rf sheaths. In Sec. III, the effective frequency concept is applied to the IED width in DF CCP. The effective frequency which is derived from the result of Sec. II is compared with that which is calculated from the particle-in-cell (PIC)/Monte Carlo (MC) simulation result. In Sec. IV, the effective frequency concept is applied to rf discharge parameters in DF CCP as it was done for the IED width in Sec. III. Based on the model of Ref. 5, several physical phenomena unique in DF CCP are found and explained in terms of the effective frequency concept. It is shown that these phenomena are attributed to the abrupt transition of the effective frequency which depends on the ratio of two driving voltages or currents. The results are summarized and discussed in Sec. V.

[a)]Author to whom correspondence should be addressed; electronic mail: jkl@postech.ac.kr

II. DESCRIPTION OF THE ANALYTIC MODEL FOR ION ENERGY DISTRIBUTIONS

The ion bombardment energy distribution on electrodes has been of much interest for researchers.[10–15] Although several models on the IED have been reported for SF CCP,[10–14] few analytic works on that have been performed for DF CCP. In this section, the analytic model for the IED in DF CCP is presented as a generalization of that in SF CCP. The IED is closely related to the ion motion in rf sheaths especially when the sheath length is much smaller than the ion mean free path. In ion-collisionless sheaths, the shape of the IED is generally bimodal and determined by the ratio of ion transit frequency f_{ion} to rf frequency f_{rf}.[13] The shape of the bimodal IED can be simply characterized as two parameters, the average ion energy and the IED width. In the low frequency limit ($f_{\mathrm{rf}} \ll f_{\mathrm{ion}}$), the IED width ΔE_i is broad since ions respond to the instantaneous rf sheath voltage. In the high frequency limit ($f_{\mathrm{rf}} \gg f_{\mathrm{ion}}$), the IED width is narrow since ions take many rf cycles to cross the sheath and respond only to the average sheath voltage. Assuming that the sheath width is constant ($=\bar{s}$) and the sheath voltage is described by

$$V_{\mathrm{sh}}(x,t) = \bar{V}_{\mathrm{sh}}(1 + \lambda F(t))x'^{(1+\nu)}, \tag{1}$$

where $x' = x/\bar{s}$ is the normalized position, $\bar{V}_{\mathrm{sh}}$ is the average sheath voltage, and ν ($\nu \neq 1$) is the scaling exponent for the dependence of the sheath electric field on the position, the equation of ion motion in the sheath is

$$\frac{d^2x'}{dt^2} = \eta(\nu+1)x'^{\nu}(1 + \lambda F(t)) \tag{2}$$

with $\eta = e\bar{V}_{\mathrm{sh}}/M\bar{s}^2$, where M is ion mass. It is assumed that the unknown function $F(t)$ consists of sinusoidal functions. From this equation, the IED can be obtained by derivation procedure similar to Ref. 14. If λ is small or if the frequency of $F(t)$ is high compared to ion transit frequency f_{ion}, the ion path is close to that corresponding to the average acceleration as follows:

$$x'(t) = \left[\frac{(1-\nu)^2}{2}\eta\right]^{1/(1-\nu)}(t-t_0)^{2/(1-\nu)}, \tag{3}$$

where t_0 is the time at which the ion enters the sheath. The substitution of Eq. (3) into Eq. (2) gives

$$\frac{d^2x'}{dt^2} = \left[\frac{(1-\nu)^2}{2}\eta\right]^{\nu/(1-\nu)}(1+\nu)[1 + \lambda F(t)](t-t_0)^{2\nu/(1-\nu)}. \tag{4}$$

The time integration yields the velocity

$$\frac{dx'}{dt} = \left[\frac{(1-\nu)^2}{2}\eta\right]^{\nu/(1-\nu)}(1+\nu) \times \int_{t_0}^{t}[1 + \lambda F(t)](t-t_0)^{2\nu/(1-\nu)}dt. \tag{5}$$

The arrival time t_1 at the electrode where $x'(t=t_1)=1$ is obtained from the average ion path of Eq. (3)

$$t_1 - t_0 = \left[\frac{(1-\nu)^2}{2}\eta\right]^{-1/2}. \tag{6}$$

From Eqs. (5) and (6), the energy of ions arriving at the electrode is therefore

$$E_i = \frac{1}{2}M\left(\frac{dx'}{dt}(t=t_1)\bar{s}\right)^2 \simeq e\bar{V}_{\mathrm{sh}}\left[1 + (2\eta)^{1/2}(1+\nu)\int_{t_1}\lambda F dt\right]. \tag{7}$$

For example, when $F(t)$ is the sinusodial function $\sin(wt)$, the ion energy is

$$E_i \simeq e\bar{V}_{\mathrm{sh}}\left[1 - \frac{\Delta E_i}{2e\bar{V}_{\mathrm{sh}}}\cos(wt_1)\right] \tag{8}$$

with

$$\frac{\Delta E_i}{e\bar{V}_{\mathrm{sh}}} = 2(1+\nu)\lambda\left(\frac{2\eta}{w^2}\right)^{1/2} = C(\nu)\lambda\frac{f_{\mathrm{ion}}}{f_{\mathrm{rf}}}, \tag{9}$$

where the coefficient is $C(\nu) = 2(1+\nu)/\pi(1-\nu)$. For example, in a dc Child law sheath ($\nu = 1/3$), the coefficient C corresponds to $4/\pi$. According to Fig. 21 of Ref. 13, the coefficient C obtained from the particle-in-cell/Monte Carlo (PIC/MC) simulation is a bit larger than $C = 4/\pi$ from the analytic model in the regime of the small $f_{\mathrm{ion}}/f_{\mathrm{rf}}$ (C is proportional to the slope in the figure). With a constant flux of ions entering the sheath, $\Gamma = dN/dt_1$, the distribution function becomes a saddle-shaped distribution with a width ΔE_i as follows:

$$f(E_i) = \frac{dN}{dE_i} = \frac{dN}{dt_1}\left(\frac{dE_i}{dt_1}\right)^{-1} = \frac{2\Gamma}{w\Delta E_i}\left[1 - \left(\frac{2}{\Delta E_i}\right)^2(E_i - e\bar{V}_{\mathrm{sh}})^2\right]^{-1/2}. \tag{10}$$

Equation (7) can also be used for IEDs in DF CCP under the assumption of the ion-collisionless sheath and the constant sheath width. When the sheath voltage is assumed to be $V_{\mathrm{sh}}(x,t) = V_{\mathrm{sh}}(t)x'^{(1+\nu)}$, the time dependence of the sheath voltage in DF CCP, $V_{\mathrm{sh}}(t)$, can be obtained from the homogeneous model for DF CCP of Ref. 5

$$V_{\mathrm{sh}}(t) = \frac{en}{2\varepsilon_0}[s_l(1 + \sin(w_l t)) + s_h(1 + \sin(w_h t))]^2. \tag{11}$$

This equation can be expressed as

$$V_{\mathrm{sh}}(t) = \bar{V}_{\mathrm{sh}}\left[1 + \lambda_l \sin(w_l t) + \lambda_h \sin(w_h t) + \frac{\lambda_l\lambda_h}{\lambda_l+\lambda_h}\sin(w_l t)\sin(w_h t) - \frac{\lambda_l^2}{4(\lambda_l+\lambda_h)}\cos(2w_l t) - \frac{\lambda_h^2}{4(\lambda_l+\lambda_h)}\cos(2w_h t)\right] \tag{12}$$

with $\lambda_{l,h}=\tilde{V}_{\mathrm{sh},l,h}/\bar{V}_{\mathrm{sh}}$, where $\tilde{V}_{\mathrm{sh},l,h}$ is the amplitude of sheath voltage oscillating with angular frequency w_l or w_h. The sheath voltage is not expressed as only the linear sum of two sinusoidal functions. It is consistent with the result of Ref. 15 that the sheath voltage with the product of two harmonic functions rather than the sum of them agrees well with the result of PIC/MC model. For the sheath voltage of Eq. (12), the function $F(t)$ in Eq. (1) corresponds to

$$\lambda F(t) = \lambda_l \sin(w_l t) + \lambda_h \sin(w_h t) + \frac{\lambda_l \lambda_h}{2(\lambda_l+\lambda_h)}[\cos(w_h t - w_l t) - \cos(w_h t + w_l t)] - \frac{\lambda_l^2}{4(\lambda_l+\lambda_h)}\cos(2w_l t) - \frac{\lambda_h^2}{4(\lambda_l+\lambda_h)}\cos(2w_h t). \tag{13}$$

Under the assumption that ion transit frequency is much smaller than the lower frequency ($f_{\mathrm{ion}} \ll f_l < f_h$), from Eq. (7), the energy of ions arriving at the electrode is

$$E_i \simeq e\bar{V}_{\mathrm{sh}}\left[1 - \frac{\Delta E_{i,l}}{2e\bar{V}_{\mathrm{sh}}}\cos(w_l t_1) - \frac{\Delta E_{i,h}}{2e\bar{V}_{\mathrm{sh}}}\cos(w_h t_1) + \frac{\Delta E_{i,f_h-f_l}}{2e\bar{V}_{\mathrm{sh}}}\sin(w_h t_1 - w_l t_1) - \frac{\Delta E_{i,f_h+f_l}}{2e\bar{V}_{\mathrm{sh}}}\sin(w_h t_1 + w_l t_1) - \frac{\Delta E_{i,2f_l}}{2e\bar{V}_{\mathrm{sh}}}\sin(2w_l t_1) - \frac{\Delta E_{i,2f_h}}{2e\bar{V}_{\mathrm{sh}}}\sin(2w_h t_1)\right] \tag{14}$$

with

$$\frac{\Delta E_{i,l,h}}{e\bar{V}_{\mathrm{sh}}} \equiv C(\nu)\lambda_{l,h}\frac{f_{\mathrm{ion}}}{f_{l,h}}, \tag{15}$$

$$\frac{\Delta E_{i,f_h\pm f_l}}{e\bar{V}_{\mathrm{sh}}} \equiv C(\nu)\frac{\lambda_l\lambda_h}{2(\lambda_l+\lambda_h)}\frac{f_{\mathrm{ion}}}{f_h \pm f_l} \tag{16}$$

and

$$\Delta E_{i,2f_l,2f_h} \equiv \frac{\lambda_{l,h}}{8(\lambda_l+\lambda_h)}\Delta E_{i,l,h}. \tag{17}$$

Assuming that two frequencies differ sufficiently ($f_h \gg f_l$), Eq. (14) can be rewritten as follows:

$$E_i \simeq e\bar{V}_{\mathrm{sh}}\left[1 - \frac{\Delta E_{i,l}}{2e\bar{V}_{\mathrm{sh}}}\left(\cos(w_l t_1) + \frac{\lambda_l}{8(\lambda_l+\lambda_h)}\sin(2w_l t_1)\right) - \frac{\Delta E_{i,h}}{2e\bar{V}_{\mathrm{sh}}}\left\{\left(1 + \frac{\lambda_l}{\lambda_l+\lambda_h}\sin(w_l t_1)\right)\cos(w_h t_1) - \frac{\lambda_l}{\lambda_l+\lambda_h}\frac{f_l}{f_h}\cos(w_l t_1)\sin(w_h t_1) + \frac{\lambda_h}{8(\lambda_l+\lambda_h)}\sin(2w_l t_1)\right\}\right]. \tag{18}$$

In the time scale of the low-frequency source, the energy of ions arriving at the electrode is given by

$$E_i \simeq e\bar{V}_{\mathrm{sh}}\left[1 - \frac{\Delta E_{i,l}}{2e\bar{V}_{\mathrm{sh}}}\cos(w_l t_1)\right]. \tag{19}$$

In the time scale of the high-frequency source, the ion energy is dependent on the phase ϕ_l of the low-frequency source

$$\begin{aligned} E_i &\simeq e\bar{V}_{\mathrm{sh}}\left[1 - \frac{\Delta E_{i,l}}{2e\bar{V}_{\mathrm{sh}}}\left(\cos\phi_l + \frac{\lambda_l}{8(\lambda_l+\lambda_h)}\sin(2\phi_l)\right) - \frac{\Delta E_{i,h}}{2e\bar{V}_{\mathrm{sh}}}\left\{\left(1 + \frac{\lambda_l}{\lambda_l+\lambda_h}\sin\phi_l\right)\cos(w_h t_1) - \frac{\lambda_l}{\lambda_l+\lambda_h}\frac{f_l}{f_h}\cos\phi_l\sin(w_h t_1)\right\}\right] \\ &\simeq e\bar{V}_{\mathrm{sh}}\left[1 - \frac{\Delta E_{i,l}}{2e\bar{V}_{\mathrm{sh}}}\cos\phi_l - \frac{\Delta E_{i,h}}{2e\bar{V}_{\mathrm{sh}}}\left(1 + \frac{\lambda_l}{\lambda_l+\lambda_h}\sin\phi_l\right)\cos(w_h t_1)\right]. \end{aligned} \tag{20}$$

III. EFFECTIVE FREQUENCY CONCEPT FOR ION ENERGY WIDTH

In Eq. (18), the ion energy has its minimum value at $w_l t_1 = w_h t_1 = 0$

$$E_{i,\min} \simeq e\bar{V}_{\mathrm{sh}}\left[1 - \frac{\Delta E_{i,l}}{2e\bar{V}_{\mathrm{sh}}} - \frac{\Delta E_{i,h}}{2e\bar{V}_{\mathrm{sh}}}\right]. \tag{21}$$

The ion energy has its maximum value at $w_l t_1 = w_h t_1 = \pi$

$$E_{i,\max} \simeq e\bar{V}_{\mathrm{sh}}\left[1 + \frac{\Delta E_{i,l}}{2e\bar{V}_{\mathrm{sh}}} + \frac{\Delta E_{i,h}}{2e\bar{V}_{\mathrm{sh}}}\right]. \tag{22}$$

The total IED width ΔE_i for DF CCP can be represented as the linear sum of IED widths contributed by two rf sources

$$\Delta E_i \equiv E_{i,\max} - E_{i,\min} = \Delta E_{i,l} + \Delta E_{i,h} = C(\nu)e\left[\tilde{V}_{\mathrm{sh},l}\frac{f_{\mathrm{ion}}}{f_l} + \tilde{V}_{\mathrm{sh},h}\frac{f_{\mathrm{ion}}}{f_h}\right] \tag{23}$$

with

$$f_{\mathrm{ion}} = \frac{1-\nu}{2}(2\eta)^{1/2}. \tag{24}$$

The ratio of two IED widths, $\Delta E_{i,l}/\Delta E_{i,h} = \lambda_l w_h/\lambda_h w_l$, is given by $\tilde{V}_{\mathrm{sh},l}w_h/\tilde{V}_{\mathrm{sh},h}w_l$. Under the condition of $\tilde{V}_{\mathrm{sh},h}/\tilde{V}_{\mathrm{sh},l} \ll f_h/f_l$, since the IED width for the low-frequency source is much larger than that for the high-frequency source, the total IED width is primarily controlled by the low-frequency source. As the ratio f_h/f_l of the higher to the lower frequency is larger, the regime where the total IED width is primarily controlled by the low-frequency source widens.

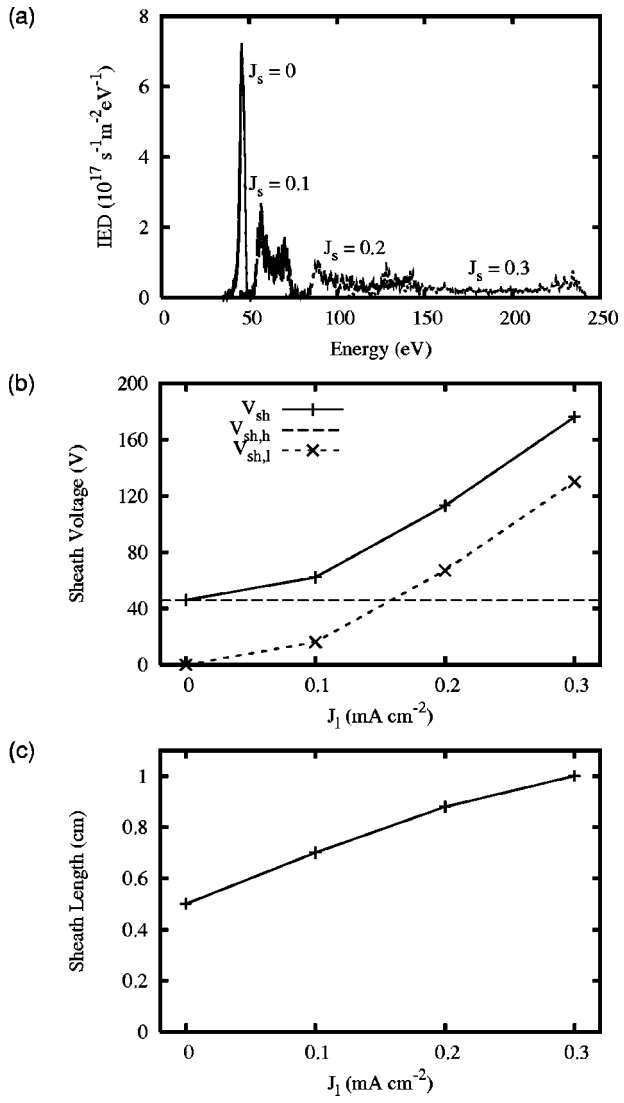

FIG. 1. PIC/MC simulation results by varying the low-frequency (2 MHz) current for the fixed high-frequency (27 MHz) current (J_h=2 mA cm^{-2}): (a) Ion bombardment energy distribution functions for various low-frequency current, (b) sheath voltages as a function of the low-frequency current, and (c) sheath length as a function of the low-frequency current.

The total IED width of Eq. (23) is symmetric for low- and high-frequency sources. We use the terms "primary" for an rf source with the fixed current or voltage and "secondary" for the other. By using Eq. (23) and the following definition for the total IED width:

$$\Delta E_i \equiv C(\nu) e \tilde{V}_{\mathrm{sh}} \frac{f_{\mathrm{ion}}}{f_{\mathrm{eff}}} \tag{25}$$

with $\tilde{V}_{\mathrm{sh}} = \tilde{V}_{\mathrm{sh},p} + \tilde{V}_{\mathrm{sh},s}$, the effective frequency for IEDs can be found

$$f_{\mathrm{eff}} = f_p \frac{1 + \tilde{V}_{\mathrm{sh},r}}{1 + \tilde{V}_{\mathrm{sh},r}/f_r} \tag{26}$$

with $\tilde{V}_{\mathrm{sh},r} = \tilde{V}_{\mathrm{sh},s}/\tilde{V}_{\mathrm{sh},p}$ and $f_r = f_s/f_p$. The IED width in DF CCP was described as that in SF CCP driven with the effective frequency. It is evident from Eq. (26) that the effective frequency is a function of the ratio of two driving frequencies and voltages. When the voltage ratio is the same as the frequency ratio, the effective frequency is

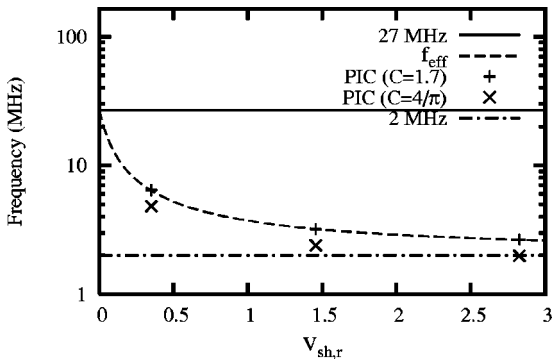

FIG. 2. Effective frequency transition for ion bombarding energy distribution functions of Fig. 1.

$$f_{\mathrm{eff}}(\tilde{V}_{\mathrm{sh},r} = f_r) = \frac{f_p + f_s}{2}. \tag{27}$$

For the fixed voltages, as the ratio f_h/f_l of the higher to the lower frequency is larger, the effective frequency is closer to the lower frequency.

For the comparison of our analytic result, one-dimensional PIC/MC simulations[16,17] without ion-neutral collisions were performed for an argon discharge at the gas pressure of 100 mTorr with the planar geometry of the gap distance of 2.5 cm. One of the electrodes was driven by the high-frequency (27 MHz) source (primary current source) with a current of 2 mA/cm^2. The other electrode was driven by the low-frequency (2 MHz) source (secondary current source). Although two current sources were applied to each electrode in our simulation, this is equivalent to applying two sources to the same electrode. Figure 1 shows argon IEDs, sheath voltages, and sheath length for various secondary currents. From the IED width, sheath voltages, and sheath length obtained by the simulation, we plotted the effective frequency f_{eff} as a function of sheath voltage ratio $\tilde{V}_{\mathrm{sh},r}$ by using Eqs. (24) and (25) for coefficients $C=1.7$ and $C=4/\pi$, as shown in Fig. 2. As the secondary current increases, the effective frequency decreases rapidly starting from the primary frequency (27 MHz) and is saturated to the secondary frequency (2 MHz). The effective frequency obtained by PIC/MC simulation with $C=1.7$ agrees better with Eq. (26) than that with $C=4/\pi$ does. This is consistent with the result of Ref. 13 that the coefficient obtained from the PIC simulation result is a bit larger than that from the analytic model, as mentioned earlier. As shown in Eqs. (24) and (25), IED widths are determined by the competition of sheath voltage, sheath length, and effective frequency. From the comparison of Figs. 1(b), 1(c), and 2, it is noted that the transition of the effective frequency, of three parameters, plays the most important role in determining the IED shape, in the regime where the secondary sheath voltage is small.

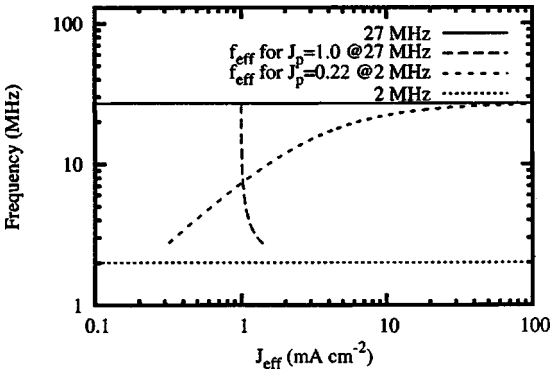

FIG. 3. Effective frequency transition for rf discharge parameters in dual rf discharges when the current of 2 or 27 MHz source varies for the fixed current of 27 or 2 MHz source to 1.0 or 0.22 mA/cm^2, respectively.

IV. EFFECTIVE FREQUENCY CONCEPT FOR DISCHARGE PARAMETERS

The quantitative definition of the effective frequency can also be obtained for rf discharge parameters as it was done for IEDs. Kim, Lee, and Shon[5] showed that rf discharge parameters for a homogeneous model of DF CCP can be expressed as those of SF CCP driven with the following effective parameters:

$$J_{\text{eff}} = \sqrt{J_p^2 + J_s^2}, \tag{28}$$

$$V_{\text{eff}} = V_p + V_s - \frac{2}{3}\frac{V_p V_s}{V_p + V_s} \tag{29}$$

and

$$f_{\text{eff}}^2(f_p, f_r, J_r) = f_p^2 \frac{1 + J_r^2}{1 + 4J_r/3f_r + J_r^2/f_r^2} \tag{30}$$

or

$$f_{\text{eff}}^2(f_p, f_r, V_r) = f_p^2 \frac{1 + (f_r V_r)^2}{(1 + V_r)\{1 + V_r - 2V_r/3(1 + V_r)\}} \tag{31}$$

with $J_r = J_s/J_p$ and $V_r = V_s/V_p$, where $J_{p,s}$ and $V_{p,s}$ are amplitudes of the rf current and rf voltage applied by the primary or secondary rf source, respectively. Since the effective frequency is determined by the competition of two rf sources, it is a function of the ratio of two driving frequencies and currents. Figure 3 shows the transition of the effective frequency from a primary frequency f_p to a secondary frequency f_s when the current of 2 or 27 MHz source varies for the fixed current of 27 or 2 MHz source to 1.0 or 0.22 mA/cm^2, respectively. As the secondary current changes, the effective frequency changes rapidly starting from the primary frequency and is saturated to the secondary frequency, like the effective frequency obtained for the IED width.

The independent control of the ion flux and the average ion bombardment energy is one of the most important issues in processing plasmas. It has been achieved by using DF CCP[2,3] where plasma density and ion bombarding energy are respectively controlled by high- and low-frequency sources. This result can be easily explained by using our model and effective frequency concept. Surendra and Graves[18] showed from their PIC/MC simulations that it was possible to independently control the ion current and energy by simultaneous manipulation of the voltage and frequency even in SF CCP. Since DF CCP can be considered as SF CCP with a variable frequency, the independent controllability of DF CCP can be deduced by using their conclusion along with the effective frequency concept. The effective current and the effective frequency in DF CCP can be independently controlled by each of two rf currents, respectively, only in an appropriate range of currents, as shown in Fig. 3. In the figure, the regime is also presented where both effective current and effective frequency vary simultaneously.

The quantitative condition for the independent control can be obtained by using the result of Ref. 5. The plasma density and average ion energy are expressed as a function of effective parameters

$$n = \frac{1}{2}\left[\frac{m(\nu_m d + 2\overline{v_e})}{e^3 u_B(\varepsilon_c + \varepsilon_e)}\right]^{1/2} J_{\text{eff}} \tag{32}$$

and

$$\overline{V} = \tfrac{3}{8} V_{\text{eff}}. \tag{33}$$

Here, m, d, and $\overline{v_e}$ are the electron mass, the length of the bulk plasma, and the electron mean speed ($=\sqrt{8eT_e/\pi m}$, where T_e is the electron temperature in unit of volts), respectively. The terms ν_m, ε_c, and ε_e are the momentum transfer frequency for electron-neutral collision, collisional loss per electron-ion pair created, and mean kinetic energy lost per electron ($=2T_e$), respectively. The term u_B is the Bohm velocity ($=\sqrt{eT_e/M}$). From Eqs. (28), (29), (32), and (33), we find the following conditions for the independent control of plasma density by the primary current and average ion energy by the secondary current:

$$J_p^2 \gg J_s^2 \quad \text{and } V_p \ll V_s. \tag{34}$$

From the relation between the primary and secondary parameters in Ref. 5

$$f_p \frac{V_p}{J_p} = f_s \frac{V_s}{J_s}, \tag{35}$$

Eq. (34) can be expressed in alternative form

$$1 \ll J_p/J_s \ll f_p/f_s \quad \text{or } 1 \ll V_s/V_p \ll f_p/f_s. \tag{36}$$

To satisfy the conditions above, the primary and secondary sources have to be high-frequency and low-frequency sources, respectively. As f_p/f_s or f_h/f_l is larger, the regime of the current or voltage for the independent control widens. A similar result was obtained from PIC/MC simulations of Ref. 8. It is also consistent with the experimental result of Kitajima *et al.*[2] where it was indicated that higher sustaining frequency makes better functional separation of biasing and sustaining voltages. However, the simple characterization of the bimodal IED structure needs the IED width as well as the average ion energy. When the result for discharge parameters is combined with that on the IED width, the following conclusion is deduced: as two frequencies differ more, the ion

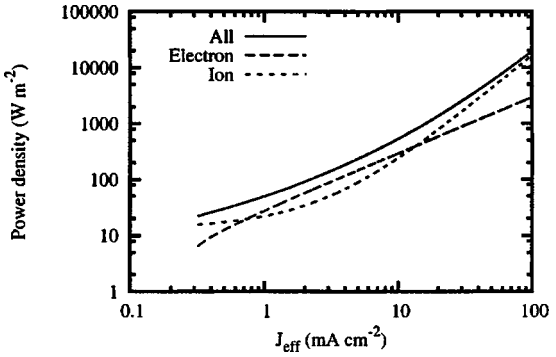

FIG. 4. Powers absorbed by electrons, ions, and all species as a function of effective current. They were obtained by varying the high-frequency (27 MHz) current for the fixed low-frequency (2 MHz) current (J_l = 0.22 mA cm^{-2}).

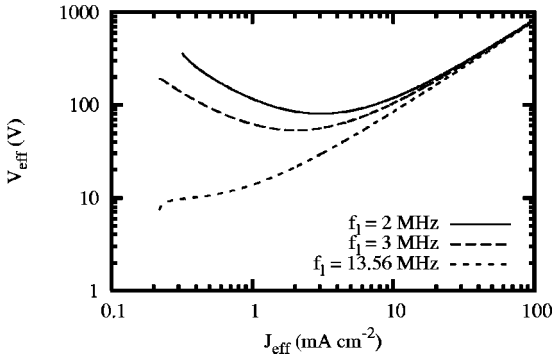

FIG. 5. Effective voltages as a function of effective current. They were obtained by varying the high-frequency (27 MHz) current for various lower frequencies with the fixed low-frequency current (J_l = 0.22 mA cm^{-2}).

flux is primarily controlled by the high-frequency source while the IED shape is primarily controlled by the low-frequency source.

Since the effective frequency is dependent on the ratio of two driving voltages or currents, physical phenomena associated with DF CCP (which cannot be observed in SF CCP) can be found. Three examples, induced by the abrupt transition of the effective frequency, are shown. The first example is double transition of mode between electron-dominated and ion-dominated power dissipations when the high-frequency (27 MHz) current changes for the fixed low-frequency (2 MHz) current (J_l = 0.22 mA cm^{-2}), as shown in Fig. 4. In SF CCP, the mode transition occurs once by varying the plasma control parameters. The ratio of ion dissipated power to electron dissipated power is proportional to the rf current and inversely proportional to the square of frequency ($P_i/P_e \propto J_{rf}/f^2$)[19]. In DF CCP, as the high-frequency current increases, both effective current and effective frequency increase (Fig. 3). Double mode transition is due to the competition of the effective current and the effective frequency. When the low-frequency (2 MHz) current of 0.22 mA cm^{-2} is applied in the absence of the high-frequency current, the ion power dominates the electron power. In the regime of the small high-frequency current (and hence small effective current), the square of the effective frequency changes more than the effective current does. Hence, the electron power increases with the high-frequency current more than the ion power does (Fig. 4). When the high-frequency current becomes sufficiently large, the mode transition from ion-dominated to electron-dominated power occurs. As the high-frequency current (and hence effective current) increases further, the effective frequency is saturated to the higher frequency (27 MHz) but the effective current increases (Fig. 3). The electron-dominated mode is changed to the ion-dominated mode in the regime of the large effective current, as shown in Fig. 4.

The second example is the negative resistance which means the decrease of the voltage with increasing the current. As shown in Fig. 5, the negative resistance is found in the regime of the small effective current, when the high-frequency (27 MHz) current changes for various lower frequencies with the fixed low-frequency current (J_l = 0.22 mA cm^{-2}). In SF CCP, the rf voltage is proportional to the rf current and inversely proportional to the square of frequency ($V_{rf} \propto J_{rf}/f^2$).[19] In DF CCP, as the high-frequency current increases, both effective current and effective frequency increase (Fig. 3). The negative resistance arises from the competition of the effective current and the effective frequency. As the high-frequency current increases, the square of the effective frequency increases more than the effective current does. As a result, the effective voltage decreases with the effective current in the regime of the small effective current, as shown in Fig. 5. As the lower frequency is smaller or two frequencies differ more, the transition of the effective frequency is more significant and hence the regime of the negative resistance widens.

The third example is the nonmonotonic behavior of plasma density versus low-frequency voltages found from PIC/MC simulations of DF CCP in Ref. 6. When the low-frequency voltage changes for the fixed high-frequency voltage, the plasma density has its local minimum value in the regime of the small low-frequency voltage. A similar result is observed in our analytic model, as shown in Fig. 6(a). It shows the plasma density as a function of the low-frequency voltage for various lower frequency with the fixed high-frequency (27 MHz) voltage (V_h = 100 V). Since this behavior is found even without considering the reduction of the bulk plasma length due to the sheath size in our other analytic modeling (not presented here), it does not seem to be attributed to the change of the sheath width, unlike the explanation of Ref. 6. To analyze this phenomenon, the plasma density was also presented as a function of the effective voltage, as shown in Fig. 6(b). In SF CCP, the plasma density is proportional to the rf voltage and the square of frequency ($n \propto V_{rf} f^2$).[19] As the low-frequency voltage increases, the effective voltage increases but the effective frequency decreases (Fig. 3). The nonmonotonic behavior of plasma density is due to the competition of the effective voltage and the effective frequency. In the regime of the small low-frequency voltage (and thus small effective voltage), the square of the effective frequency decreases abruptly with the low-frequency voltage and hence the plasma density decreases

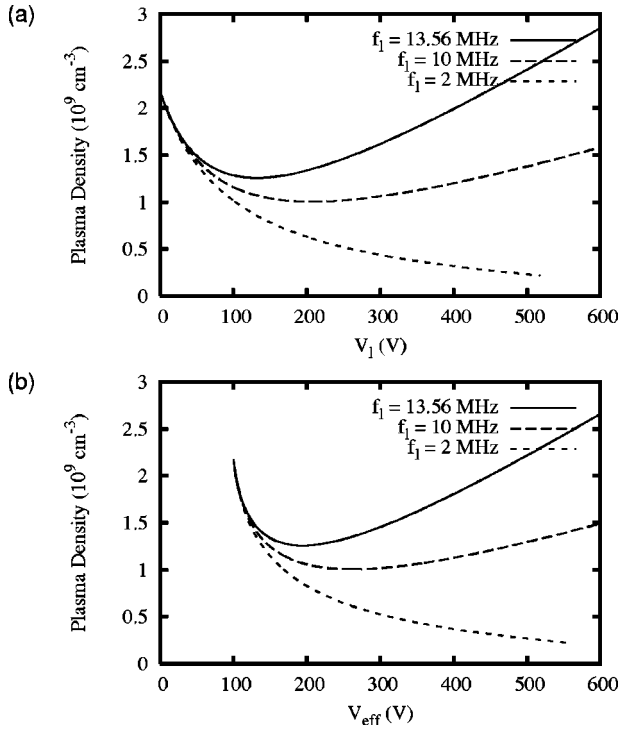

FIG. 6. Plasma densities as a function of (a) the low-frequency voltage and (b) the effective voltage for various lower frequencies with the fixed high-frequency (27 MHz) voltage (V_h=100 V).

with the effective voltage, as shown in Fig. 6(b). As the low-frequency voltage increases further, the effective frequency is saturated to the lower frequency (2 MHz) but the effective voltage increases (Fig. 3). As a result, the plasma density increases with the effective voltage in the regime of the large effective voltage, as shown in Fig. 6(b). As the lower frequency is smaller or two frequencies differ more, the transition of the effective frequency becomes more significant and hence the regime where the plasma density decreases widens.

V. CONCLUSIONS

We have proposed a concept of effective frequency to enhance our understanding of DF CCP, which can be considered as SF CCP driven with effective parameters. It was shown that this concept is useful to explain several physical issues associated with DF CCP. The concept was applied to both ion bombardment energy distribution functions and rf discharge parameters in DF CCP. The quantitative definition of the effective frequency for the IED width was obtained by analyzing ion dynamics in ion-collisionless dual rf sheaths. It was found that the effective frequency transition plays an important role in determining the IED function in DF CCP. It also explains the possibility of independent control of ion flux and ion bombardment energy in DF CCP only under certain plasma parameter regimes which are given by our theoretical results. As two frequencies differ more, the ion flux and the IED shape are primarily controlled by the high-frequency and low-frequency sources, respectively. Several physical phenomena unique in DF CCP were also found, such as double transition between electron-dominated and ion-dominated mode, the negative resistance, and the nonmonotonic behavior of plasma density. They were explained using scaling laws along with the effective frequency concept. It was shown that these phenomena are attributed to the abrupt transition of the effective frequency which depends on the ratio of two driving voltages or currents. Although we showed only a few examples where the effective frequency concept is applied, the concept can have many wider applications. For different applications or models, different quantitative definitions of the effective frequency are required. Our concept of effective frequency in a dual frequency system can be generalized to a multiple frequency system. It can also be applied to any shape of current or voltage by using Fourier transforms.

ACKNOWLEDGMENTS

Helpful discussions with Dr. J. W. Shon at the Lam Research Corporation, Dr. M. S. Hur at the University of California at Berkeley, Dr. N. Yu. Babaeva, and Dr. O. V. Manuilenko are greatly acknowledged. This work was supported in part by the Lam Research Corporation, Samsung Electronics, and Teralevel Nano Devices Project, 21c Frontier R&D Program in Korea Ministry of Science and Technology.

[1]T. Makabe and K. Maeshige, Appl. Surf. Sci. **192**, 176 (2002).
[2]T. Kitajima, Y. Takeo, Z. L. Petrovic, and T. Makabe, Appl. Phys. Lett. **77**, 489 (2000).
[3]H. H. Goto, H.-D. Lowe, and T. Ohmi, IEEE Trans. Semicond. Manuf. **6**, 58 (1993).
[4]S. Rauf and M. J. Kushner, IEEE Trans. Plasma Sci. **27**, 1329 (1999).
[5]H. C. Kim, J. K. Lee, and J. W. Shon, Phys. Plasmas **10**, 4545 (2003).
[6]J. K. Lee, N. Babaeva, H. C. Kim, O. Manuilenko, and J. W. Shon, IEEE Trans. Plasma Sci. **32**, 47 (2004).
[7]H. C. Kim and J. K. Lee, Phys. Rev. Lett. **93**, 085003 (2004).
[8]P. C. Boyle, A. R. Ellingboe, and M. M. Turner, J. Phys. D **37**, 697 (2004).
[9]C. Kittel, *Introduction to Solid State Physics*, 7th ed. (Wiley, New York, 1996).
[10]P. Benoit-Cattin and L. C. Bernard, J. Appl. Phys. **39**, 5723 (1968).
[11]A. Metze, D. W. Ernie, and H. J. Oskam, J. Appl. Phys. **65**, 993 (1989).
[12]C. Wild and P. Koidl, Appl. Phys. Lett. **54**, 505 (1989).
[13]E. Kawamura, V. Vahedi, M. A. Lieberman, and C. K. Birdsall, Plasma Sources Sci. Technol. **8**, R45 (1999).
[14]W. J. Goedheer, Plasma Sources Sci. Technol. **9**, 507 (2000).
[15]V. Georgieva, A. Bogaerts, and R. Gijbels, Phys. Rev. E **69**, 026406 (2004).
[16]C. K. Birdsall, IEEE Trans. Plasma Sci. **19**, 65 (1991).
[17]J. P. Verboncoeur, M. V. Alves, V. Vahedi, and C. K. Birdsall, J. Comput. Phys. **104**, 321 (1993).
[18]M. Surendra and D. B. Graves, Appl. Phys. Lett. **59**, 2091 (1991).
[19]M. A. Lieberman and A. J. Lichtenberg, *Principles of Plasma Discharges and Materials Processing* (Wiley, New York, 1994).